

Received June 25, 2016, accepted July 12, 2016, date of publication July 19, 2016, date of current version August 26, 2016.

Digital Object Identifier 10.1109/ACCESS.2016.2592941

# Upper-Bound on Dose Reduction in CT Reconstruction for Nodule Detection

RUBEN DE MAN<sup>1</sup>, GE WANG<sup>1</sup>, (Fellow, IEEE), MANNUDEEP K. KALRA<sup>2</sup>, ALEXI OTRAKJI<sup>2</sup>, SCOTT HSIEH<sup>3</sup>, AND NORBERT PELC<sup>3</sup>

<sup>1</sup>Department of Biomedical Engineering, Rensselaer Polytechnic Institute, Troy, NY 12180, USA

<sup>2</sup>Department of Radiology, Massachusetts General Hospital, Boston, MA 02114, USA

<sup>3</sup>Department of Radiology, Stanford University, Stanford, CA 94305, USA

Corresponding author: R. De Man (rubendeman@gmail.com)

**ABSTRACT** The success of X-ray computed tomography (CT) as a widespread medical diagnosis tool has led to concerns about possible harm due to the increased average radiation dose to the population. A highly effective way to reduce CT radiation dose is to use iterative image reconstruction. All major CT vendors now offer iterative reconstruction solutions and claim that they can achieve the desired image quality at only a fraction of the dose level needed with conventional filtered backprojection (FBP) reconstruction. In this paper, we empirically estimate the upper bound on the achievable dose reduction in CT reconstruction in the context of a clinical detection task. We do this based on a series of patient lung CT data sets, with and without nodules, for a large number of random noise realizations. We analyze lesion detectability in the FBP images, in which case performance is lost due to the sub-optimal reconstruction. We compare this to lesion detectability directly in the raw data domain, where by definition, all information is still available with specific location information. This, therefore, represents the best scenario any reconstruction algorithm could achieve from raw data without additional prior information. The results indicate that a threefold dose reduction is feasible relative to FBP reconstruction: specifically, the upper bound on dose reduction was estimated at 62.5% for 90% detection accuracy and 66.2% for 80% detection accuracy. Statistical weighting is responsible for approximately half of that benefit.

**INDEX TERMS** Computed tomography, radiation dose, cancer.

## I. INTRODUCTION

X-ray computed tomography (CT) has become an essential tool for detecting and diagnosing abnormalities within the body. It has become one of the safest and most effective ways for medical doctors to examine their patients and ensure their health. Because of this, the many applications of CT have seen widespread implementation in hospitals and clinics in the past four decades. A relatively new application is the early detection of lung nodules. Lung cancer is one of the most prevalent and deadly cancers, claiming the lives of millions of people annually [1]. Detecting it early is crucial to cure or treat the cancer properly [2]. Early lung cancers often present in the form of non-calcified pulmonary nodules. CT is ideally suited to detect these nodules, since it creates high-contrast images that can reveal small lesions in great detail. However, prior studies have raised safety concerns over the widespread use of CT because of its radiation dose [3]. Other studies claim that the so-called Linear No-Threshold Model is invalid and the concerns are

unjustified [4]. Nevertheless, tremendous efforts have been made to limit radiation dose to the patient in accordance with the ALARA principle, which maintains that radiation doses to patients should be kept “as low as reasonably achievable” [5].

The main challenge with reducing CT radiation dose is the corresponding increase in image noise. It is also known that lesion detectability depends on image noise. Hence, simply reducing CT dose could negatively impact diagnostic performance. Traditional reconstruction algorithms based on filtered backprojection (FBP) are suboptimal in terms of their noise versus dose tradeoff. Many improved reconstruction techniques have been proposed that enable dose reduction while maintaining a certain image quality or noise level. Especially, iterative reconstruction (IR) algorithms have been widely studied and appear to offer substantial noise reduction, thereby enabling reduction in radiation dose [6]–[10]. Given the large variety of IR algorithms proposed and the equally large number of evaluation methodologies used in

their studies, it is not clear what the fundamental dose reduction entitlement is of the best possible CT reconstruction algorithm. Research has shown that task-based assessments of image quality are preferred, as simplified metrics based on image noise and spatial resolution could lead to incorrect conclusions [11], [12]. The number of IR approaches is tremendous: every vendor offers one or more commercial IR algorithms, many research groups have presented their own preferred IR algorithms, and new approaches continue to be presented. The recent AAPM Low Dose CT Grand Challenge [13] is an attempt at comparing a large number of approaches in a clinically meaningful evaluation framework.

We are interested in estimating an upper-bound on CT reconstruction dose reduction or a lower-bound on dose required for a given imaging task [14]. The raw sinogram data contains all the measured information about the patient. Any processing steps may convert that information into a format that is more accessible to human observers or image analysis tools, but they don't generate any new patient-specific information. The reconstruction algorithm will lose some of that information or at best maintain that information, but can never create new independent information. Hence, a sinogram domain analysis can serve as the best case scenario, requiring the lowest dose possible to perform the task. In a recent study [15], the potential for dose reduction was determined for a quantification task, in which the density of a lesion was estimated using the raw sinogram data and FBP images respectively. In the same spirit of the work reported in [15], our paper aims to analyze the dose reduction opportunity relative to FBP, but for a detection task instead of a quantification task. In addition, we restrict our analysis to real clinical images and lung nodules. For this purpose, we use a number of patient lung CT datasets and compare lesion detectability in the raw data domain and in the image domain. To estimate the true upper-bound, the sinogram domain analysis is optimized by taking into account the statistical uncertainty on each individual measurement due to x-ray quantum noise and detector electronic noise. This optimal estimation is compared to the standard clinical practice using the FBP images. The rationale of this study is that any possible IR algorithm will try to improve upon FBP by better translating the information available in the raw sinogram data into the reconstructed IR images, also trying to take into account the statistical uncertainty in the measurements. The best we can possibly hope for IR to perform (without additional prior information) is as well as the raw data domain. Hence this study estimates an upper bound on IR dose reduction.

## II. METHODS

This study consists of an image generation step and a lung nodule detection step. The image generation step uses real patient lung CT images with nodules, image processing to create virtual CT images without nodules, CT simulations at various dose levels to generate a large number of noise realizations, and FBP reconstruction. The lung nodule

detection is performed in both the sinogram domain and the image domain by computing the similarity of the noisy test data to the noise-free benchmark. Receiver operating characteristic (ROC) curves are generated to quantify detection accuracy as a function of radiation dose. Each of these steps is explained in detail in the following subsections.

### A. PATIENT IMAGES

This study is based on clinical CT images of the thorax for 21 adult patients. The image database consists of standard dose chest CT scans with multiple nodules in each scan. Because of this, it was important to ensure that there was only one nodule in each slice. This constraint was implemented to avoid the confounding effects that could be caused by the presence of multiple nodules. 28 lung nodules were selected from these 21 scans for evaluation in the current study. The nodules ranged from 5.0 mm to 10.0 mm in diameter. For each of these lung nodules, the original image served as the “nodule present” case. In order to obtain corresponding “nodule absent” patient images, we performed image processing to “erase” the lung nodules but maintaining otherwise identical images. This was done by replacing the nodule region with a neighboring lung tissue region in an effort to make the new background as realistic as possible in the absence of the original voxel values. Using this method, images with and without lung nodules were generated for all clinical cases. These images were defined as the ground-truth images. Even though the images have some low-level noise since they are real clinical images, we defined these images as noise-free for the purpose of this study. Example benchmark images for three patients are shown in Figure 1.

### B. CT SIMULATION AND RECONSTRUCTION

Sinograms were re-generated using the Computer Assisted Tomography Simulator (CatSim) software [16]. The geometry was based on a 64-channel multidetector-row CT scanner (GE Lightspeed VCT, GE Healthcare, Waukesha, WI) using 888 detector cells spaced by 1.024 mm, a source-to-isocenter distance of 541 mm, a source-to-detector distance of 949 mm, the large bowtie filter, a monochromatic 70keV spectrum, and 984 views over a full 0.5s rotation. Each of the 28 different clinical images and their nodule-free counterparts were used to simulate noise-free sinograms, which were then reconstructed via 2D fan-beam FBP. Reconstructions were performed using a  $512 \times 512$  matrix with 0.8 mm pixel size, corresponding to a 40 cm field-of-view. These noise-free sinograms and FBP images serve as benchmark in the classification of the noisy test sinograms and FBP images.

Poisson noise was approximated by adding scaled Gaussian noise to the log-converted sinograms

$$p = \hat{p} + G\left(\frac{1}{\sqrt{I}}\right) \quad (1)$$

where  $\hat{p}$  is the noise-free sinogram,  $p$  is the noisy sinogram,  $G(\sigma)$  is random Gaussian noise with standard deviation  $\sigma$ ,

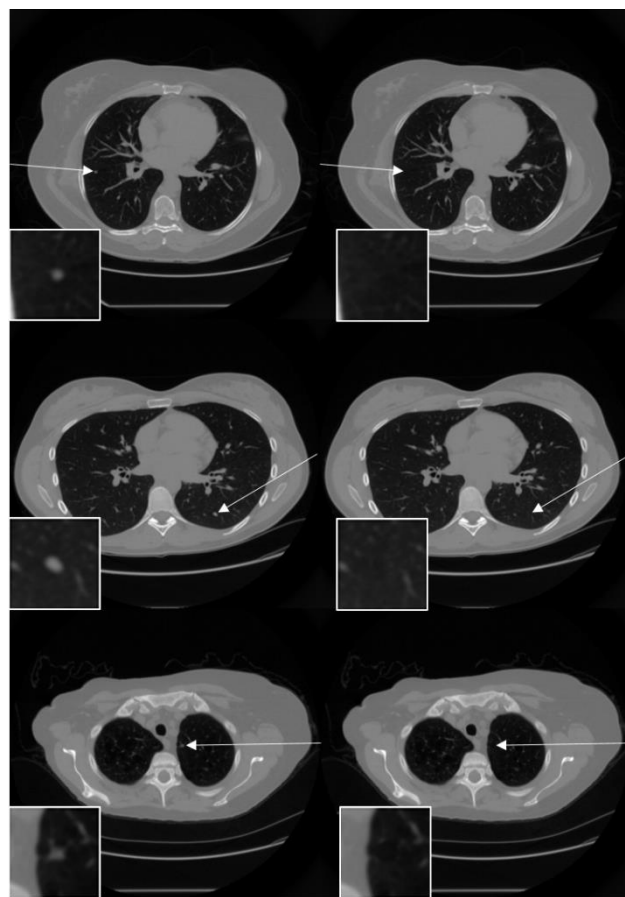


**FIGURE 1.** Examples of clinical images with (left) and without (right) nodules. The arrows point to the nodule and where the nodule was erased, respectively. The inset images are zoomed versions of the corresponding regions. The display interval is  $[0, 0.4] \text{ cm}^{-1}$ .

and  $\hat{I}$  is the transmitted scan scaled in the number of x-ray photons. No detector electronic noise was included. Eight different dose levels were used corresponding to tube

currents [0.00625, 0.0125, 0.025, 0.05, 0.1, 0.2, 0.4, and 0.8] mA or integrated tube currents of [0.003125, 0.00625, 0.0125, 0.025, 0.05, 0.1, 0.2, and 0.4] mAs, which are lower than realistic clinical protocols as well as those reported in the published literature for detection of lung nodules [17]. This is an empirical way to explore the lower-bound of radiation dose for lung nodule detectability. 100 noise realizations were generated for each dose level and for each of the 28 clinical images, with and without lung nodules, resulting in a total of 44,800 sinograms and images.

### C. LUNG NODULE DETECTION

In order to perform the detection task, the noisy test data sets were compared to the noise-free “nodule present” and “nodule absent” data sets. This methodology (presented schematically in Figure 2) assumes that the observer has complete knowledge of what the data set should look like with versus without a lung nodule and needs to estimate whether the noisy test dataset is closer to the “nodule present” or “nodule absent” data set. For both the sinogram domain detection task and the image-domain detection task, we use a *normalized similarity metric* defined as

$$\text{NSM} = \frac{\langle (w \cdot b - w \cdot a), (w \cdot x - w \cdot a) \rangle}{\|w \cdot b - w \cdot a\|^2} \quad (2)$$

where all data sets are represented as vectors,  $a$  is the data without lung nodule,  $b$  is the data with lung nodule,  $x$  is the test data,  $w$  is a weighting vector,  $\langle , \rangle$  is the inner product between two vectors. Geometrically, this projects the test vector  $x$  onto the sub-space spanned by the benchmark vectors  $a$  and  $b$ . The NSM gives the normalized coordinate of  $x$  in that sub-space: ideally 0 in the absence of a lung nodule and 1 in the presence of a lung nodule. However, due to the noise, a continuous distribution of NSM values is obtained. As the noise level increases, the NSM may no longer correctly decide whether a nodule was present or not, since errors grow

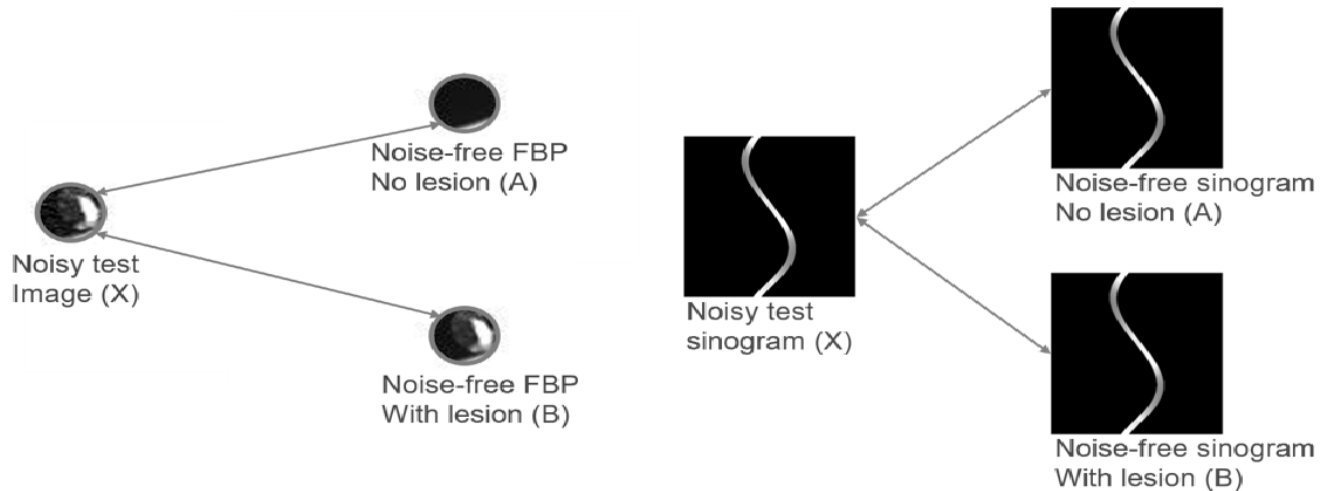


**FIGURE 2.** The lung nodule detection process consists of comparing the noisy test data to the two noise-free benchmarks. This process can be performed in the image domain (left) or in the sinogram domain (right).

larger in the detection task. For image-domain analysis, the weight factor  $w$  is a binary mask image corresponding to the circular region around the nodule, eliminating influence of the noise outside the region on the NSM. For the same reason the sinogram domain analysis uses a binary mask sinogram as weight factor, which is based on the reprojection of the image mask, as illustrated in Figure 3.



**FIGURE 3.** Mask image (left) and mask sinogram (right) used to limit the region over which the normalized similarity metric compares the test data to the benchmark data.

In the sinogram domain analysis, the weight sinogram  $w$  may also include a statistical weighting factor, to take into account the different degrees of uncertainty in each measurement corresponding to the varying noise standard deviation, as given by

$$w_{SINO} = m_{SINO} * \sqrt{\hat{I}} \quad (3)$$

where  $m$  is the binary mask sinogram,  $\hat{I}$  is the estimated sinogram measurement and  $\sqrt{\hat{I}}$  is the standard deviation of the measurement, assuming a Poisson distribution.

#### D. ROC ANALYSIS

The decision concerning whether a test case includes a lesion or not is based on a threshold on the NSM metric. If the threshold is set low, there is a risk of obtaining too many false positives (poor specificity). If the threshold is set high, there is a risk of obtaining too many false negatives (poor sensitivity). ROC curves are commonly used to analyze the relationship between sensitivity and specificity for all possible threshold values [18]. The area under the curve (AUC) is typically used to represent the overall detection accuracy. For each dose level, the NSM scores for all clinical cases were combined, and a single ROC curve was derived, with a single AUC. We could then analyze the AUC as a function of dose level, and draw conclusions about the potential level of dose reduction.

### III. RESULTS AND DISCUSSION

Figure 4 shows an example of a clinical test data set. The left side shows the original clinical image (in this case with lesion) and the simulated noise-free sinogram. The right side shows the sinogram after noise insertion and the corresponding FBP reconstruction.

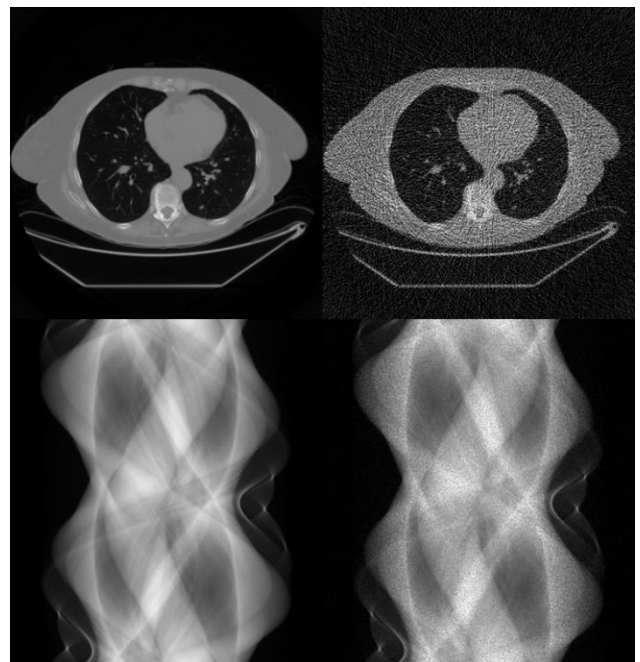


**FIGURE 4.** Examples of images and sinograms used in the analysis without (left) and with (right) noise. The display intervals for the images and the sinograms are  $[0, 0.4] \text{ cm}^{-1}$  and  $[0, 6]$  respectively.

Figure 5 shows the NSM results for all 44,800 test cases, for the FBP images, the sinograms without statistical weighting and the sinograms with statistical weighting. The plus signs represent the cases with lesions and the circles represent the cases without lesions. The horizontal axis represents the dose level. We staggered the cases with and without lesions to better visualize all cases where they would overlap. As expected, at higher dose levels the NSM scores are grouped around 0 (no lesion) and 1 (with lesion), with little or no overlap. As the dose level decreases, the spread on the NSM scores increases and the distributions start to overlap. One can already note a reduced spread in the sinogram domain compared to the image domain, particularly with the inclusion of statistical weighting.

To better visualize the NSM distributions, Figure 6 shows the NSM results using box plots, for all 44,800 test cases, for the FBP images, the sinograms without statistical weighting and the sinograms with statistical weighting. The black lines represent the cases with lesion and the gray lines represent the cases without lesions. Again, at higher dose levels the NSM scores are grouped around 0 (no lesion) and 1 (with lesion), with little or no overlap. As the dose level decreases, the spread on the NSM scores increases and the distributions start to overlap. One can now more easily observe the reduced spread in the sinogram domain case, particularly with the inclusion of statistical weighting.

Figure 7 shows the combined ROC curves for all clinical cases at different dose levels, for the FBP images, the sinograms without statistical weighting and the sinograms with statistical weighting. No color coding was used, but

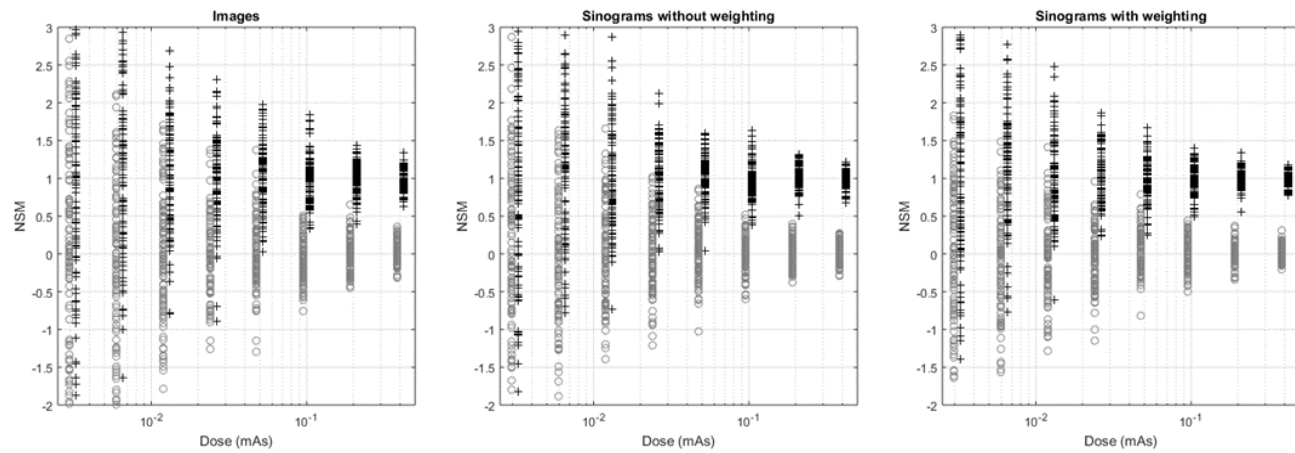


**FIGURE 5.** Scatter plots showing the NSM values at various dose levels for the FBP analysis and the sinogram analysis without and with statistical weighting. Plus signs represent cases with lesions and circles represent cases without lesions.

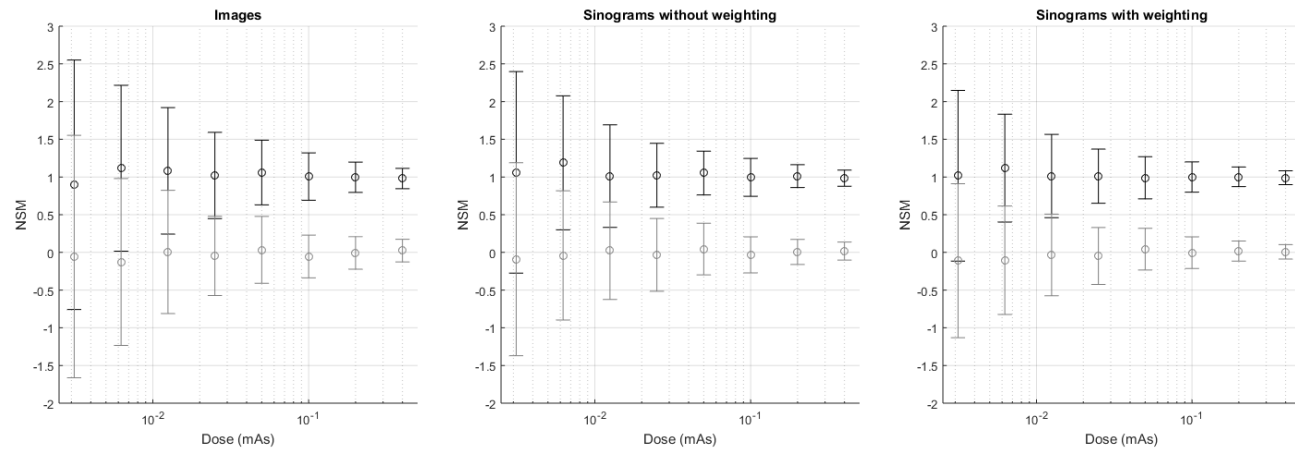


**FIGURE 6.** Box plots showing the NSM values at various dose levels for the FBP analysis and the sinogram analysis without and with statistical weighting. Black lines represent cases with lesion and gray lines represent cases without lesion.

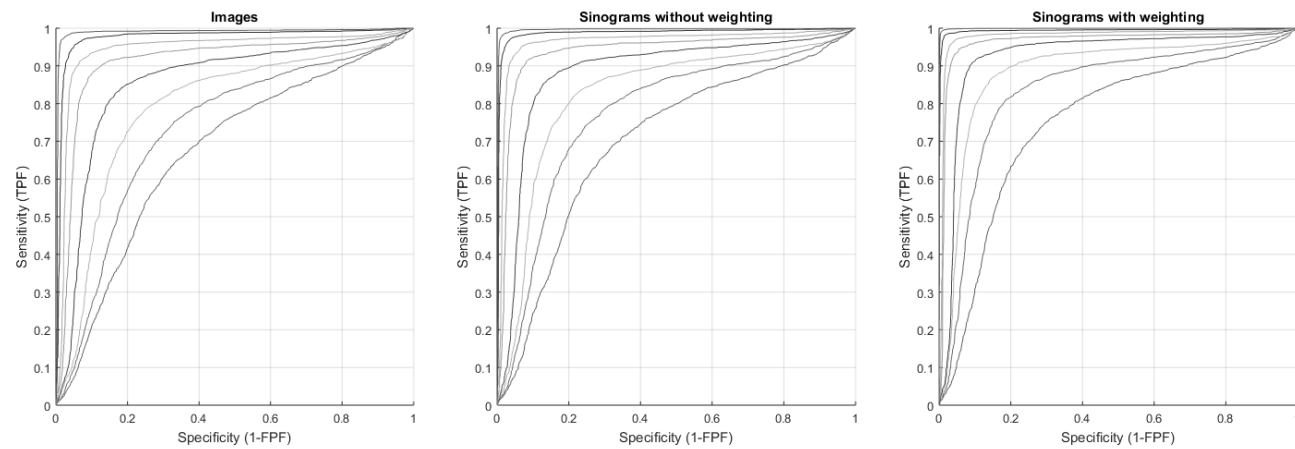


**FIGURE 7.** Combined ROC curves for the FBP analysis and the sinogram analysis without and with statistical weighting. The different curves correspond to different dose levels from 0.003125 mAs (curves with lowest AUC) to 0.4 mAs (curves with highest AUC).

the lowest ROC curves correspond to the lowest dose levels and the highest ROC curves correspond to the highest dose levels. As expected, the area under the curve (AUC) increases with dose level, and it can be noted that the ROC curves are

improved for the sinogram domain analysis, particularly with statistical weighting.

Figure 8 shows the AUC as a function of dose level on a logarithmic scale, for the FBP analysis and sinogram

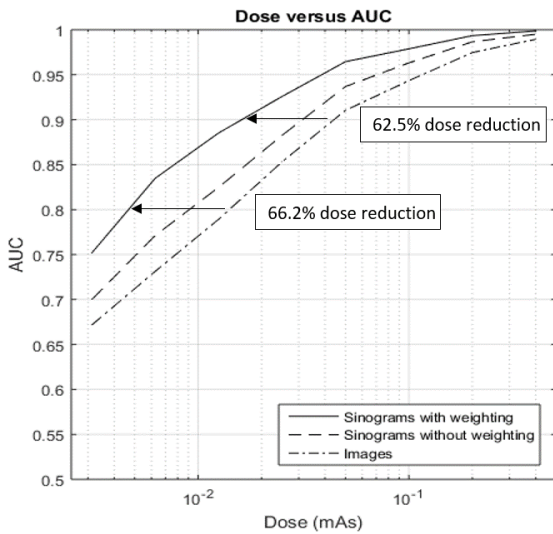


**FIGURE 8.** AUC as a function of dose level on a logarithmic scale, for the FBP analysis and sinogram analysis without and with statistical weighting.

analysis without and with statistical weighting. The AUC approaches 0.5 for the lowest doses and 1 for the highest dose levels. The AUC curves can be used to identify the level dose reduction to achieve a fixed detection accuracy. 90% accuracy could be achieved using approximately 0.09mA (FBP), 0.06mA (sinogram without statistical weighting) and 0.03mA (sinogram with statistical weighting). 80% accuracy could be achieved using approximately 0.03mA (FBP), 0.02mA (sinogram without statistical weighting) and 0.01mA (sinogram with statistical weighting). The corresponding dose reduction of the sinogram analysis is approximately 1/3 and 2/3, without and with weighting.

This study has some limitations: we use a relatively simple noise model (noise is added after the logarithm and no electronic noise is included), we perform the reconstructions in 2D (to avoid confounding physics effects such as beam hardening and scatter), and we do not study the increased performance that some reconstruction algorithms may offer by including prior knowledge, which could result in even higher dose reduction levels. Nevertheless, the results clearly show how much raw data information is lost (and therefore dose is wasted) by FBP reconstruction as well as the importance of statistical weighting. A practical implication of this study is that a reconstruction algorithm can be evaluated based on whether its dose reduction approaches the upper-bound computed here. Claims of even higher dose reduction may not be valid in the absence of any additional prior information.

The intention of this paper was to empirically study the dose reduction entitlement for an idealized detection task. While this study analyzes the limit of detectability, radiologists may prefer not to operate at these extremely low dose levels in clinical practice. First, the assumption that the benchmarks with and without lesion are exactly known is not valid in practice. Second, sufficient image quality is also needed to provide contextual information and make

the images easier to read. Finally, improved image quality may be important to increase radiologist confidence and effectiveness.

#### IV. CONCLUSION

We estimated a fundamental upper-bound on reconstruction-based CT dose reduction for a detection task. We used clinical lung CT images with and without nodules to generate sinograms at a range of dose levels and we performed FBP reconstruction. The detection task was performed in the image domain, as well as in the sinogram domain, with and without statistical weighting. To perform the lung nodule detection task, we defined a metric to compare the test data to the ground truth benchmarks and to decide on the presence or absence of a nodule. We analyzed the detection accuracy as a function of detection domain (image or sinogram) and dose level. As expected, the sinogram domain detection performed systematically better than the image-domain detection. The upper-bound on dose reduction without statistical weighting was estimated to be approximately threefold. The upper-bound on dose reduction with statistical weighting was estimated at 62.5% for 90% detection accuracy and 66.2% for 80% detection accuracy. These results are consistent with the results presented in [15], where a dose reduction of 64% was estimated for a quantification task. While the ultra-low dose levels used in this study may not be practical, the results are an indication of the highest possible dose reduction that any reconstruction algorithm could possibly achieve compared to FBP for a nodule detection task.

#### REFERENCES

- [1] *World Cancer Report 2003*, accessed on Jun. 25, 2016. [Online]. Available: <http://www.iarc.fr/en/publications/pdfs-online/wcr/2003/index.php>
- [2] C. F. Mountain, "Revisions in the international system for staging lung cancer," *Chest*, vol. 111, no. 6, pp. 1710–1717, 1997.
- [3] B. F. Wall, G. M. Kendall, A. A. Edwards, S. Bouffler, C. R. Muirhead, and J. R. Meara, "What are the risks from medical X-rays and other low dose radiation?" *Brit. J. Radiol.*, vol. 79, no. 940, pp. 285–294, 2014.
- [4] J. A. Siegel, C. W. Pennington, B. Sacks, and J. S. Welsh, "The birth of the illegitimate linear no-threshold model: An invalid paradigm for estimating risk following low-dose radiation exposure," *Amer. J. Clin. Oncol.*, Nov. 2015.
- [5] K. N. Prasad, W. C. Cole, and G. M. Haase, "Radiation protection in humans: extending the concept of as low as reasonably achievable (ALARA) from dose to biological damage," *Brit. J. Radiol.*, vol. 77, no. 914, pp. 97–99, 2004.
- [6] J. Xu, M. K. Fuld, G. S. K. Fung, and B. M. W. Tsui, "Task-based image quality evaluation of iterative reconstruction methods for low dose CT using computer simulations," *Phys. Med. Biol.*, vol. 60, no. 7, p. 2881, 2015.
- [7] H.-W. Tseng, J. Fan, M. A. Kupinski, P. Sainath, and J. Hsieh, "Assessing image quality and dose reduction of a new X-ray computed tomography iterative reconstruction algorithm using model observers," *Med. Phys.*, vol. 41, no. 7, p. 071910, 2014.
- [8] S. W. Lee et al., "Image quality assessment of ultra low-dose chest CT using sinogram-affirmed iterative reconstruction," *Eur. Radiol.*, vol. 24, no. 4, pp. 817–826, Apr. 2014.
- [9] S. Singh et al., "Adaptive statistical iterative reconstruction technique for radiation dose reduction in chest CT: A pilot study," *Radiology*, vol. 259, no. 2, pp. 565–573, 2011.
- [10] C. Schabel et al., "Clinical evaluation and potential radiation dose reduction of the novel sinogram-affirmed iterative reconstruction technique (SAFIRE) in abdominal computed tomography angiography," *Acad. Radiol.*, vol. 20, no. 2, pp. 165–172, Feb. 2013.

- [11] H. H. Barrett, K. J. Myers, C. Hoeschen, M. A. Kupinski, and M. P. Little, "Task-based measures of image quality and their relation to radiation dose and patient risk," *Phys. Med. Biol.*, vol. 60, no. 2, pp. R1–R75, 2015.
- [12] E. Samei and S. Richard, "Assessment of the dose reduction potential of a model-based iterative reconstruction algorithm using a task-based performance metrology," *Med. Phys.*, vol. 42, no. 1, pp. 314–323, 2015.
- [13] *Low Dose CT Grand Challenge*, accessed on Jun. 25, 2016. [Online]. Available: <http://www.aapm.org/GrandChallenge/LowDoseCT/>
- [14] J. Y. Vaishnav, W. C. Jung, L. M. Popescu, R. Zeng, and K. J. Myers, "Objective assessment of image quality and dose reduction in CT iterative reconstruction," *Med. Phys.*, vol. 41, no. 7, p. 071904, 2014.
- [15] S. S. Hsieh, D. A. Chesler, D. Fleischmann, and N. J. Pelc, "A limit on dose reduction possible with CT reconstruction algorithms without prior knowledge of the scan subject," *Med. Phys.*, vol. 43, no. 3, pp. 1361–1368, 2016.
- [16] B. De Man et al., "CatSim: A new computer assisted tomography simulation environment," *Proc. SPIE*, vol. 6510, p. 65102G, Mar. 2007.
- [17] H. Rusinek et al., "Pulmonary nodule detection: Low-dose versus conventional CT," *Radiology*, vol. 209, no. 1, pp. 243–249, 1998.
- [18] H. H. Barrett, C. K. Abbey, and E. Clarkson, "Objective assessment of image quality. III. ROC metrics, ideal observers, and likelihood-generating functions," *J. Opt. Soc. Amer. A*, vol. 15, no. 6, pp. 1520–1535, 1998.



**RUBEN DE MAN** is currently pursuing a high school diploma at Shenendehowa High School, Clifton Park, NY, USA. The research presented in this paper was conducted during a research internship with the Rensselaer Polytechnic Institute in collaboration with Stanford University and Harvard Medical School. He is currently an Intern with the Massachusetts General Hospital. His work is focused on improving the detection and treatment of lung cancer and other diseases of the chest. His general research interests include X-ray computed tomography, thoracic imaging, and cardiac imaging.



**GE WANG** (F'03) received the Ph.D. degree in electrical and computer engineering, where he is the Clark and Crossan Endowed Chair Professor and Director of the Biomedical Imaging Center/Cluster, Rensselaer Polytechnic Institute, Troy, NY, USA. He wrote the pioneering papers on the first spiral cone-beam CT algorithm (1991 and 1993). He and his collaborators published the first paper on bioluminescence tomography, creating a new area of optical molecular tomography. He authored over 400 journal papers, which are highly cited. His group published the first papers on interior tomography and omni-tomography for grand fusion of all relevant tomographic modalities (all-in-one) to acquire different datasets simultaneously (all-at-once) with simultaneous CT-MRI as an example. His group has been in close collaboration with world-class groups, and continuously well-funded by federal agents. Spiral/helical cone-beam/multislice CT imaging is constantly used in almost all hospitals worldwide. There are over 85 million CT scans yearly in USA alone, with a majority in the spiral cone-beam/multislice mode. His expertise includes X-ray computed tomography, optical molecular tomography, multimodality imaging, and deep learning. He is the lead Guest Editor of four IEEE TRANSACTIONS MEDICAL IMAGING special issues on X-ray CT, molecular imaging, compressive sensing, and spectral CT respectively, the founding Editor-in-Chief of the *International Journal of Biomedical Imaging*, Associate Editor of IEEE TRANSACTIONS MEDICAL IMAGING, MEDICAL PHYSICS. He is a fellow of the SPIE, OSA, AIMBE, AAPM, and AAAS. His results were featured in nature, science, and PNAS, and recognized with various academic awards.



**MANNUDEEP K. KALRA** has been with the International Atomic Energy Agency to develop extensive teaching resources related to CT radiation dose for the developing nations. He is currently a Radiologist of the Divisions of Thoracic and Cardiac Imaging with the Massachusetts General Hospital and Associate Professor of Radiology with the Harvard Medical School. He is also the Director of the MGH Webster Center for Advanced Radiation Research and Education. His main areas of research interests include CT radiation dose optimization, CT technology development, and dual energy CT. He has authored over 250 original research, reviews, and book chapters in his research fields. He has edited three textbooks related to Multidetector CT and CT Radiation Dose. He has also won several prizes and awards for his research papers and educational exhibits in area of his key areas of interest.



**ALEXI OTRAKJI** is currently a Post-Doctoral Research Fellow with the Division of Thoracic Radiology, Massachusetts General Hospital and Harvard Medical School. His main area of research interests include dual energy CT applications in thoracic imaging, CT radiation, and contrast volume reduction. He has participated in many quality and safety related projects in radiology.



**SCOTT HSIEH** received the Ph.D. degree in electrical engineering from Stanford University. He is an Instructor with Stanford University. He has been with the Ultrasound and Solid State Physics. His current projects include dynamic filtration of X-ray beams, next-generation detector hardware, and improved reconstruction algorithms. His research interests include improving the image quality and dose efficiency in computed tomography scanners.



**NORBERT PELC** received the B.Sc. degree from the University of Wisconsin-Madison, where he has been involved in the interface of technology, engineering, and biomedicine and the Ph.D. and master's degrees in medical radiological physics from Harvard University. He is currently the Chair of the Department of Bioengineering. His current interest focuses on computed tomography, with a specialization in methods to improve the information content and image quality and to reduce the radiation dose from these examinations. His primary research interests include physics, engineering, and mathematics of diagnostic imaging and the development of applications of this imaging technology. He served on the first National Advisory Council of the National Institute of Biomedical Imaging and Bioengineering, National Institutes of Health. He is a member of the National Academy of Engineering, and a fellow of the American Association of Physicists in Medicine, the International Society for Magnetic Resonance in Medicine, and the American Institute of Medical and Biological Engineering.